Pflügers Arch – Eur J Physiol (1997) 434:830–840

INSTRUMENTS AND TECHNIQUES

A.H. Gitter · M. Bertog · J.-D. Schulzke · M. Fromm

Measurement of paracellular epithelial conductivity by conductance scanning

Received: 10 February 1997 / Received after revision: 9 June 1997 / Accepted: 10 June 1997

Abstract A new method, conductance scanning, allows determination of local para- and transcellular conductivities in flat epithelia. Experiments were performed on kidney distal tubule cells, MDCK clone C11, which form monolayers on permeable supports. Above the apical surface, local voltage drops generated by a sinusoidal current clamp were recorded by means of a scanning microelectrode. Data were collected above cell centres and tight junctions. The scanning signal was always significantly higher above the tight junctions, but was uniformly distributed along the junctions. For determination of conductivities two procedures were applied. Method 1: the supraepithelial potential distribution was computed for given trans- and paracellular currents at all positions of the electrode. In a fit algorithm, the currents were varied until the calculated potential difference equalled the voltage measured. Method 2: after collecting scanning data in control Ringer's, intercellular space width was reduced by mucosal addition of 40 mM sucrose and a second set of data was obtained at decreased paracellular, but presumably unchanged transcellular, conductivity. From these data, trans- and paracellular conductivities were calculated. Results of both methods were in excellent agreement. Confluent MDCK-C11 monolayers exhibited a transepithelial conductivity of 13 mS/cm^2. The transcellular pathway contributed 2.6 mS/cm^2 (20%) and the paracellular pathway 10.5 mS/cm^2 (80%) to the total conductivity. Collapse of the lateral intercellular spaces decreased the paracellular conductivity to 4 mS/cm^2 (60%). Confluent MDCK-C11 monolayers constitute true "leaky" epithelia with homogeneously distributed trans- and paracellular conductivities. In conclusion, conductance scanning fills a methodical gap, which hitherto impeded the functional characterzation of tight junctions.

Key words MDCK-C11 cells · Tight junction · Local conductance

A.H. Gitter · M. Bertog · M. Fromm (✉)
Institut für Klinische Physiologie,
Universitätsklinikum Benjamin Franklin, Freie Universität Berlin,
D-12200 Berlin, Germany

J.D. Schulzke
Medizinische Klinik I: Gastroenterologie und Infektiologie,
Universitätsklinikum Benjamin Franklin, Freie Universität Berlin,
D-12200 Berlin, Germany

Introduction

Many pathophysiological processes in epithelia are accompanied, maintained or even caused by defects of the transepithelial barrier [2, 6, 7, 12, 25, 29]. Evidence has accumulated showing that these originate from an increase of tight-junction permeability, which is controlled intracellularly. Furthermore, an increasing body of circumstantial evidence indicates the important physiological role of regulated paracellular transport processes. Hence, there is a clear demand for a quantitative differentiation of trans- and paracellular conductivities in epithelia.

In many recent papers the transepithelial resistance ("TER") or its reciprocal equivalent, the transepithelial conductivity (G^e), is used as an indicator of junctional barrier characteristics. However, TER represents an overall measure of the whole exposed area of the experimental chamber. Since TER consists of a paracellular and a transcellular resistance in parallel, it is also affected by transcellular resistance. Further, TER is altered if cell cultures exhibit imperfect confluency or sealing.

We have, therefore, developed a method that allows determination of trans- and paracellular conductivities in flat epithelial domains. The new method is based on the analysis of local differences in current density which are recorded in the supraepithelial bath solution with a stepping and scanning glass microelectrode during application of a transepithelial clamp current. Since the inhomogeneous conductivity of an epithelium is evaluated, the method is called conductance scanning. With this, we have investigated clone C11 of Madin-Darby Canine Kidney cells (MDCK-C11), which functionally and mor-

phologically resembles the intercalated cells of renal collecting ducts [19, 32, 34].

Theoretical considerations

As in previous voltage-scanning studies [5, 10] a scanning microelectrode measured voltage differences that reflect different current densities in the supraepithelial bath solution. The local differences in current density are caused by the inhomogeneous conductivity in the adjacent cell layer.

For the sake of comparability, the voltage difference (ΔV) measured across the excursion of the microelectrode (Δx) was transformed into the "apparent conductivity" (G_A), i.e. the local difference in current density divided by the transepithelial voltage:

$$G_A=(\Delta V/\Delta x)/(\rho \cdot V^e) \quad (1)$$

where ρ is the specific resistivity of the electrolytic bath solution, and V^e is the transepithelial voltage, corrected for the contribution produced by the voltage drop across the saline and the cell culture support of the monolayer. All conductivities are referred to the gross tissue area, which is equal to the aperture of the Ussing chamber holding the tissue.

Each epithelial area recorded from was characterized by two local conductivities in parallel, the transcellular (G^c) and the paracellular (G^p) conductivity, the sum of which equals the local epithelial conductivity (G^e) [10]. G^c and G^p contribute to the apparent trans- and paracellular conductivities measured (G_A^c and G_A^p) according to:

$$G_A^c=G^c+k_1 \cdot G^p \quad (2)$$

and

$$G_A^p=G^c+k_2 \cdot G^p, \quad (3)$$

with k_1 and k_2 being parameters (dependent on the geometrical configuration) that describe the contribution of the inhomogeneous electric field caused by G^p at the spot recorded from. The uniform transcellular conductivity, G^c, contributes equally to the electric field above cells and junctions, because the area occupied by tight junctions is very small as compared to the gross tissue area.

Materials and methods

Cell culture and Ussing chamber

Visual observation with high resolution is needed in order to allow exact positioning of the scanning microelectrode. Since the tissue is illuminated through the cell culture support, good optical quality of the support is crucial. Therefore, we chose Cellagen CD 24 culture plate inserts (ICN Biomedicals, Aurora, Ohio, USA), which are made of pepsin-solubilized collagen and are permeable, highly transparent, thin (0.1 mm when bathed in Ringer's) and flexible. Owing to the material's low density, its resistance is relatively low. MDCK cells of the C-11 clone in the 60th to 70th passage were plated on Cellagen supports and cultured as described by Gekle et al. [11] i.e. under standard conditions (37° C, air with 5% CO_2) in Minimum Essential Medium with Earle's salts, amino acids, *N*-acetyl-L-glutamine, and 2.2 g/l $NaHCO_3$ (MEM FG0325, Biochrom, Berlin, Germany) which was supplemented with 10% fetal calf serum, 100 units/ml penicillin and 100 µg/ml streptomycin (Biochrom). Confluent monolayers were investigated after 3–4 days of cultivation.

The collagen support of the monolayer was fixed onto a flat nylon ring by means of Histoacryl tissue glue (Braun Melsungen, Germany). The preparation was then mounted horizontally, mucosal surface up, in a Lucite four-electrode Ussing-type chamber. The exposed area was 5.7 mm². Serosal and, near the epithelium, mucosal half-chamber were cylindrical with a diameter of 6 mm. The upper part of the chamber widened to a diameter of 10 mm, in order to facilitate horizontal movements of the scanning and reference electrodes (see below) introduced into the mucosal half-chamber. To allow for visual control of the epithelium and the position of the scanning electrode, the upper and lower apertures of the chamber were closed with glass coverslips. The distance between the upper coverslip and the mucosal surface of the epithelium was 8.5 mm, that between the lower coverslip and the serosal face of the collagen support was 5 mm. Transepithelial current was passed through a pair of silver wire electrodes (outer diameter 1 mm, coated with AgCl), which were mounted at the bottom and top of the chamber. While the serosal current electrode was circular (inner diameter 4 mm), the mucosal one was U-shaped to provide a lateral opening through which scanning and reference electrodes were introduced. Both half-chambers were continuously perfused at a rate of 2–4 ml/min with bathing solution that was oxygenated with a mixture of 95% O_2 and 5% CO_2 and was kept at 37° C. The composition of control Ringer's solution (in mM) was: 123 NaCl, 28 $NaHCO_3$, 4 KCl, 1.7 $CaCl_2$, 1 KH_2PO_4, 0.9 $MgCl_2$, 10 D(+)-glucose, pH 7.6 was adjusted by addition of 0.8–0.9 mM NaOH; in hyperosmolar solution 40 mM sucrose had been added to control Ringer's.

Experimental set-up

The Ussing chamber was mounted horizontally on a precise, manually controlled electrically driven micromanipulator (Mod. 5171, Eppendorf, Hamburg, Germany) that was firmly attached to the stage of an upright microscope (Axioplan, Carl Zeiss Jena, Germany). The preparation was observed by video microscopy using a long-distance object lens (×20/0.4, Zeiss) and subsequent magnification (Optovar ×1.25–×2.5, Zeiss). A digital image processor (Argus 10, Hamamatsu) allowed on-screen determination of the centre of the area of apical cell membrane and measurement of the distance to neighbouring cell centres. An AC bridge system with synchronous demodulation was used to measure above the epithelium the potential gradients generated by a sinusoidal current of 24 Hz and 20 µA. Potential differences were measured differentially with a reference and a scanning electrode, both made of borosilicate glass capillaries (No. 1403515, Hilgenberg, Malsfeld, Germany). The glass microelectrodes were shaped using a microforge and filled with 0.5 M saline; they had input resistances of 4–5 MΩ. The scanning electrode, directed almost vertically towards the epithelial surface, was placed close above the epithelium using a micromanipulator. The reference electrode was kept at a constant position 200–300 µm above the epithelium. With fixed electrodes, the spot on the monolayer to be recorded from was brought to the scanning electrode by moving the Ussing chamber with the electrically driven micromanipulator. For each spot recorded from, the origin of the vertical axis (i.e. the axis perpendicular to the epithelial plane) was defined by lifting the epithelium until it barely touched the recording electrode, as indicated by disturbances in the electrical signal derived from the electrode. If visible damage of the epithelium or a sudden increase in the scanning signal occurred while touching the surface, the recordings were discarded. In order to avoid damage during recording, the epithelium was lowered, away from the electrode, by three vertical steps (0.17 µm each) of the micromanipulator. After positioning the scanning electrode, it was moved stepwise up and down (vertical excursion Δx=10 µm, frequency 0.7 Hz) by means of a piezoelectric driver attached to the electrode holder.

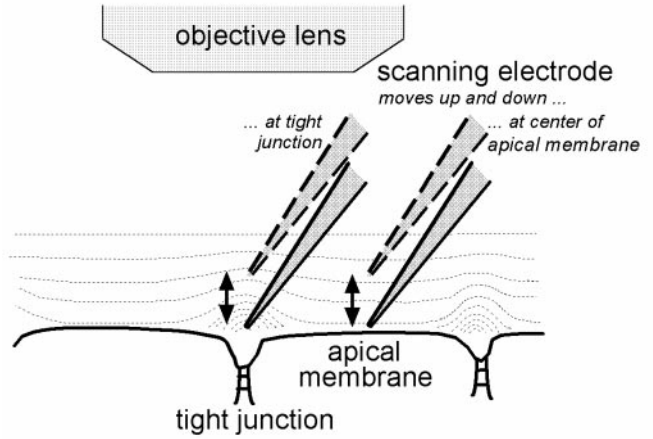

Fig. 1 Cartoon of conductance scanning principle. The transepithelial clamp–current induced voltage drops as illustrated by isopotential lines above the epithelium. The voltage drog, ΔV, was measured at the tight junction or centre of the apical cell membrane as the difference between the two potentials across the excursion of the scanning microelectrode

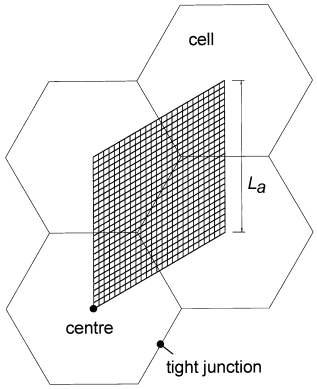

Fig. 2 In the fixed geometry of a two-dimensional hexagonal array of cells, a rhombus ("surface cell") of the size of a single cell's apical surface was defined and its area was divided into 25×25 elements ("surface elements"). The rhombus' side had a length, L_a, equal to the distance between the centres of neighbouring apical cell membranes

Measurement

The local voltage drop, ΔV, was measured as the difference between the two voltages recorded at the ends of the vertical steps of the scanning electrode (Fig. 1). With a signal integration time of 1 min, the sensitivity was 1 mS/cm^2; the resolution of the voltage drop measured was limited by the spatial resolution achieved in positioning the scanning electrode. V^e was measured with Ag/AgCl electrodes linked to the drainage lines for the mucosal and serosal baths by KCl-agar bridges. The voltage drop across the saline and the collagen support of the monolayer was subtracted. In each experiment, the scanning signals ($\Delta V/\Delta x$) were measured in one area, (1) above the centres of three to four adjoining cells, and (2) above three to four tight junctions of the these cells, before and after addition of sucrose to the mucosal bath solution. More precisely, the tight-junction recording sites were in the middle between the corners where three cells meet. Control experiments were performed in order to test the influence of stimulus amplitude on transepithelial resistance and the scanning signal. The contribution of capacitive transepithelial currents was investigated with the transepithelial AC-impedance technique, used as described previously [9]. All values are given as mean±SEM, n refers to the number of monolayers investigated. The unpaired t-test was used to determine the significance of differences; $P<0.05$ was considered significant.

Mathematical models

In order to enable recognition of systematic errors caused by model assumptions, three different mathematical models were employed to derive trans- and paracellular conductivities.

Method 1 assumed a fixed geometry of a two-dimensional hexagonal array of cells describing the mucosal surface of the epithelium. In detail, the geometrical representation comprised a rhombus of the size of an apical cell surface, including half of the intercellular spaces. This area was called surface cell (Fig. 2). Translational symmetry of the epithelial surface was assumed. At some distance from the epithelial surface, significant potential differences between different points in a plane parallel to the surface must disappear. This distance, L_b, was called bulk cell height. The rhombohedron formed by the surface cell and the bulk height was called bulk cell. Each side of the surface cell had a lengt, L_a, that equalled the distance between the centres of the apical cell membranes of adjoining cells. The length L_a was subdivided into n_a parts and thus the surface cell fell into $n_a \cdot n_a$ surface elements. (In order to achieve stable fits, division into $n_a \cdot n_a$=25 · 25 elements was required). The bulk cell height L_b was divided into n_b=$n_a \cdot L_b/L_a$ parts, and thus the bulk cell fell into $n_a \cdot n_a \cdot n_b$ rhomboid bulk elements. (The reason for this choice is explained in the Appendix). The glass electrode was considered as a rod (outer diameter 1.7 μm) that pointed vertically at the epithelial surface with its tip being 0.5 μm distant from the surface. For each position of the scanning electrode (i.e. 0.5 and 10.5 μm above the tight junction and above the centre of the cell's apex), bulk elements occupied by the electrode were listed.

In general, each bulk element had six faces, through which current might flow to adjoining elements. (If, however, the adjoining element was occupied by the glass electrode rather than Ringer's solution, there was no current through this face of the bulk element). Numerical analysis allowed computation of the supraepithelial potential distribution for given trans- and paracellular currents at all positions of the electrode. The currents were varied until the calculated potential difference equalled the difference measured between top and bottom positions of the scanning electrode. Division of the trans- and paracellular currents thus derived by the V^e measured yielded G^c and G^p. The numerical solution to the field problem is shown in the Appendix. Calculations were carried out on a PC using an algorithm programmed in Fortran (Fig. 3).

Method 2 was based on a selective perturbation of G^p: the intercellular spaces were collapsed by an osmotic gradient (mucosal addition of 40 mM sucrose) and thus G^p was decreased. Signals were recorded close above cells and junctions, and also at 30 μm above the epithelium, in order to calculate (using Eq. 1) the apparent transepithelial conductivity of the epithelial area explored (G^e_A). The set of experimental data, together with linear Eqs. 2 and 3, allowed computation of the conductivities G^c, G^p and G^e:

Upon mucosal addition of sucrose, G^c should remain constant:

$$G^c\,[1] = G^c\,[2], \tag{4}$$

where the states without and with sucrose are denoted by [1] and [2], respectively. The change of G^e_A of the area explored is equal to the change of G^p:

$$G^e_A\,[2] - G^e_A\,[1] = G^p\,[2] - G^p\,[1] \tag{5}$$

Using Eqs. 2–5, the parameters k_1 and k_2 of Eqs. 2 and 3 can be calculated from G^c_A, G^p_A and G^e_A measured:

$$k_1 = (G^c_A\,[2] - G^c_A\,[1])/(G^e_A\,[2] - G^e_A\,[1]) \tag{6}$$

and

$$k_2 = (G^p_A\,[2] - G^p_A\,[1])/(G^e_A\,[2] - G^e_A\,[1]) \tag{7}$$

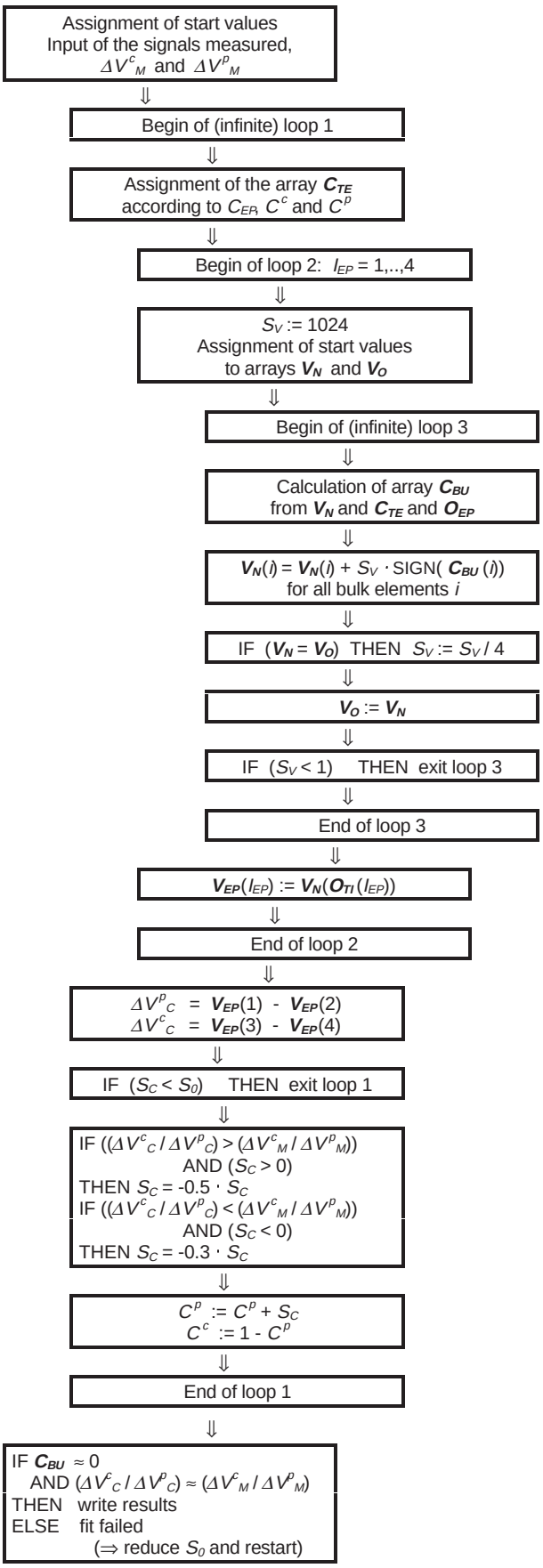

With the result of Eqs. 6 and 7, Eqs. 2 and 3 allow the calculation of

$$G^p[1]=(G^p_A[1]-G^c_A[1])/(k_2-k_1) \quad (8)$$

$$G^p[2]=(G^p_A[2]-G^c_A[2])/(k_2-k_1) \quad (9)$$

and

$$G^c[1]=G^c[2]=G^c_A[1]-k_1 G^p[1] \quad (10)$$

G^e is the sum of trans- and paracellular conductivities,

$$G^e[1]=G^c[1]+G^p[1] \quad (11)$$

$$G^e[2]=G^c[2]+G^p[2] \quad (12)$$

The difference between G^e and G^e_A reflects the net contribution of currents from epithelial areas other than that from which the recording was made.

Method 3 assumed a constant value of G^c in all recording areas. Elimination of G^p in Eq. 2 (by means of Eq. 3) resulted in a linear relation between G^p_A and G^c_A:

$$G^c_A=(1-k_1/k_2)\,G^c+(k_1/k_2)\,G^p_A \quad (13)$$

This model allowed computation of G^c from the regression lines, but G^p could not be determined. The conductivity of the epithelial area explored (G^e_A) was not required.

Results

Requirements for the experimental procedure were studied in a theoretical analysis. Control experiments were performed to exclude the possibility of alterations induced by the AC current applied. Without and with an osmotic gradient across the epithelium, scanning signals, expressed as apparent conductivities, were measured above cell centres and tight junctions. From these data, trans- and paracellular conductivities and the superposition of trans- and paracellular currents were determined using the mathematical models.

Fig. 3 Flow chart of the fit algorithm. Three-dimensional arrays represent the supraepithelial potential in all bulk elements (V_N and V_O) and the net current flowing into each bulk element (C_{BU}). In a set of three-dimensional arrays (forming a four-dimensional array, O_{EP}), bulk elements containing glass electrode are indicated for all positions of the electrode (index I_{EP}). The coordinates of the electrode's tip opening are stored in a separate array (O_{TI}). The transepithelial current depends on the length of tight junction in each surface element, and is described in a two-dimensional array (C_{TE}). The potential at the electrode's tip is stored for all positions of the electrode in a one-dimensional array (V_{EP}). At the beginning of the fit loop, an educated guess of the transepithelial current (C_{EP}) and the relative contributions of trans- and paracellular currents (C^c and C^p) is used. For all four positions of the electrode, the potential in each bulk element is varied until the net current flowing through the six faces of the element vanishes. Above cell centre and above tight junction, the voltage across the excursion of the electrode's tip is calculated from the potential field computed. These voltages (ΔV^c_C and ΔV^p_C) are compared to the voltages measured (ΔV^c_M and ΔV^p_M). Trans- and paracellular currents (C^c and C^p) are then changed, and again the corresponding potential field is computed and compared with the voltages measured. This procedure is continued until C^c and C^p are determined with sufficient precision ($S_c<S_o$)

Theoretical analysis

In order to know how close the scanning electrode must approximate the epithelium to distinguish between trans- and paracellular pathways, supraepithelial potential distributions were computed using the algorithms of model 1. By plotting the electric potential against the distance from the tight junction on the line connecting two neighbouring cell centres, electric potential profiles were obtained at different distances from the surface of a leaky epithelium (Fig. 4). Within a few micrometres from the surface, significant field distortions near the tight junctions allowed clear discrimination of junctions and cells. This was not the case, however, at 10 μm or more above the surface; therefore, approaching the surface to ≤3 μm is advisable. Near the tight junction the electric potential as a function of distance from the surface becomes highly non-linear. A caveat is thus necessary in the interpretation of signal changes, because they may originate from variations in the distance between the electrode and the surface.

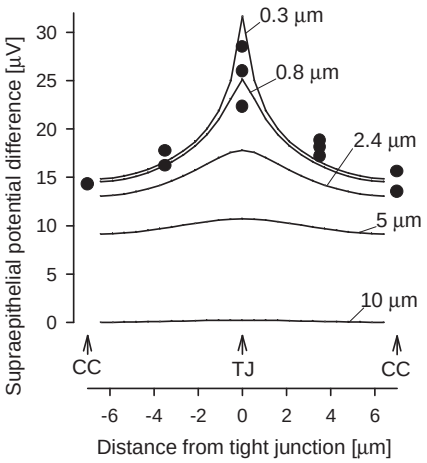

Fig. 4 Computation of the electric potential generated above an epithelium of hexagonal cells by a transepithelial current of 400 μA/cm² (*solind lines*). Paracellular pathways were assumed to contribute 0.8 to the conductivity. The abscissa indicates distance from tight junction (*TJ*) on the line connecting two neighbouring cell centers (*CC*), which are 13.33 μm apart. The zero-potential point was chosen 10 μm above the cell centre. The curves correspond to different distances from the surface: *a*: 0.3 μm; *b*: 0.8 μm; *c*: 2.4 μm; *d*: 5 μm; *e*: 10 μm. *Symbols* show a series of measurements over cell centres, tight junction and intermediate locations, performed in a single experiment on the line connecting two neighbouring MDCK cells

Upon an arbitrary ±10% variation of the mean distance between neighbouring cells (13.3 μm, see below) the calculated results varied by ±45% (G^c under control conditions), +15% and −13% (G^c in the presence of an osmotic gradient), −8% and +11% (G^p under control conditions), or −9% and +11% (G^p in the presence of an osmotic gradient). (If $G^c << G^p$, G^c became relatively sensitive to the variation of cell distance). Thus, it is necessary to choose epithelial areas of regular cellular geometry, to measure cell distances, and to average the results obtained.

In order to establish the requirements for sensitivity, the relationship between the precision of the potential gradients, measured 0.5 and 10.5 μm above the epithelial surface, and the accuracy of the paracellular conductivity derived was evaluated (Fig. 5). Transepithelial current was confined to 400 μA/cm². When the paracellular conductivity ranged from 0 to 100%, the signal measured above the cell centers decreased from 22 to 15 μV while above simple tight junctions it increased from 22 to 39 μV and above intersections of the junctions of three neighbouring cells it increased from 22 to 41 μV (Fig. 5A). For instance, a 10% difference in leakiness resulted in respective changes in ΔV of −0.7 μV above cell centres, 1.7 μV above tight junctions, and 1.9 μV above intersections of junctions. A prerequisite for quantification of the paracellular conductivity is thus a sensitivity of ≤1 μV. Note that even if the transcellular pathways were non-conductive, the signal measured above the cell centres would still be 38% of that above tight junctions (Fig. 5B).

Morphology and transepithelial resistances

In saline the filter support (Cellagen CD 24) was completely transparent allowing visual control of the experiment. The resistance of the support without cells in control Ringer's was 2–3 Ω · cm². Microscopic observation of the preparation revealed epithelial areas of a perfectly

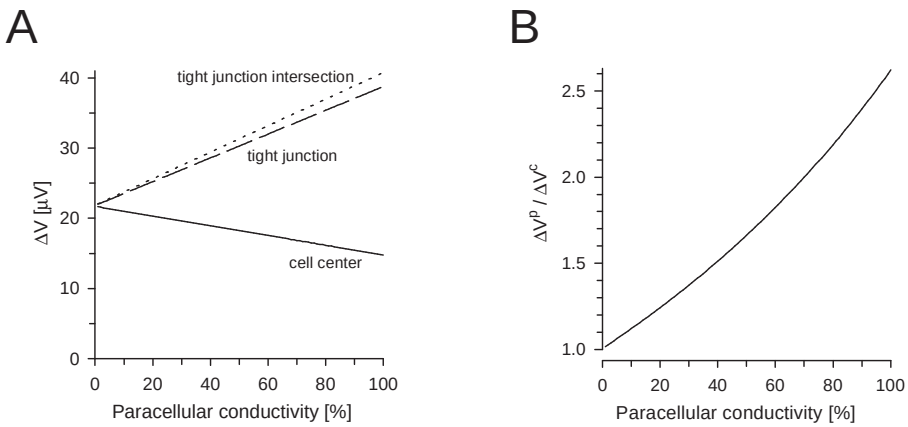

Fig. 5 **A** Computation of conductance-scanning signals in relation to leakiness: (1) above cell centres (*solid line*); (2) above tight junctions (*dashed line*); and (3) above intersections of the junctions of three neighbouring cells (*dotted line*). *Abscissa* shows the fraction of paracellular to overall epithelial conductivity; *ordinate* is the signal measured with the electrode (ΔV). **B** Fraction of the scanning signal above the tight junction to the signal above the cell centre ($\Delta V^p/\Delta V^c$), in relation to leakiness

confluent monolayer and spots with damaged cells and probably loss of confluence. The experiments were restricted to areas of perfect confluence and approximately hexagonal cells. The transcepithelial resistance, as measured with conductance scanning electrodes, was 83±6 Ω · cm² (*n*=10) when determined using model 1, and 71±7 Ω · cm² (*n*=10) when determined with model 2.

The mean distance between neighbouring cell centres was 13.3±0.5 μm (*m*=21 measurements on *n*=10 tissues). (It decreased with prolonged cultivation). In control Ringer's, the cell borders were clearly visible, indicating dilated intercellular spaces (Fig. 6A). In order to determine how flat the surface was, the heights of neighbouring cell centres and the intermediate tight junctions were measured by recording the vertical position of the scanning electrode when it barely touched the surface. The difference in height between neibhbouring cell centres was 1.79±0.33 μm (*m*=18, *n*=2). The tight junction was 2.0±0.5 μm (*m*=10, *n*=2) lower than the centre of the apical cell membrane.

After mucosal addition of 40 mM sucrose, cell borders became less pronounced, but remained visible (Fig. 6B). The transepithelial resistance of undamaged confluent areas was 161±10 Ω · cm² (*n*=10) and 137±13 Ω · cm² (*n*=10) when determined with models 1 and 2, respectively.

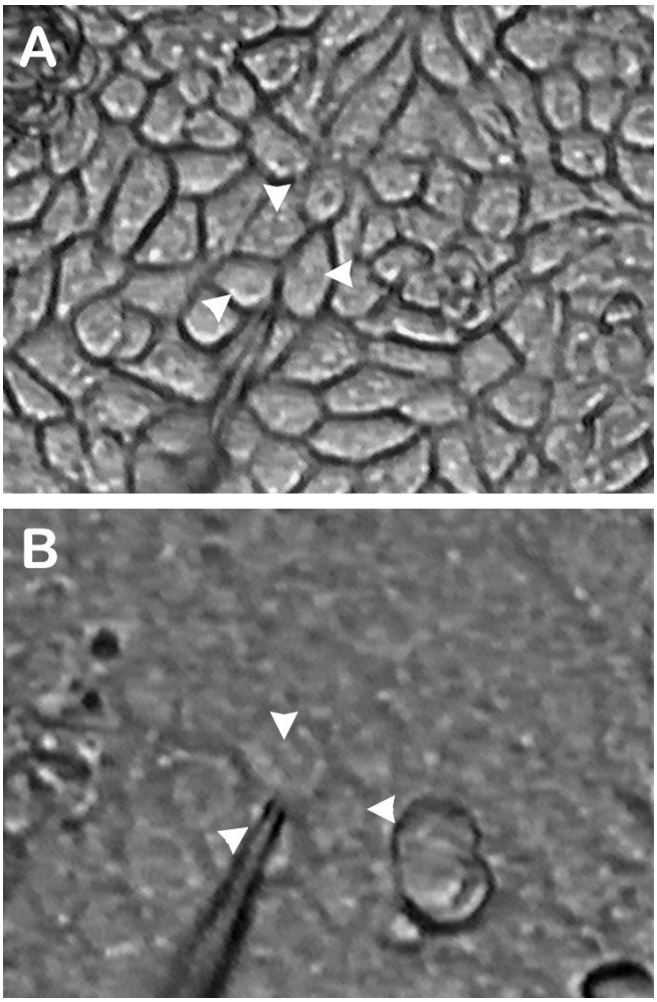

Fig. 6 Light micrographs showing the mucosal surface of an MDCK-C11 monolayer before (**A**) and after (**B**) addition of 40 mM sucrose to the mucosal Ringer's. Note that the border lines separating individual cells became less pronounced, indicating collapse of lateral intercellular spaces. *Arrows* indicate the cells from which recordings were made

Control experiments

Control experiments were performed to exclude the possibility that the epithelial conductivities recorded were affected by the current applied. The current/voltage curves measured with transepithelial electrodes were linear in the range of 0–50 μA, corresponding to 0–1 mA/cm² (Fig. 7A). Similarly, the scanning signal (Δ*V*) was linear in the same range (Fig. 7B). Being in the range of currents tested, the amplitude of the transepithelial current applied during conductance scanning does not affect the conductivities measured.

By using alternating current, polarization effects were avoided, but the contribution of reactive components due to membrane capacitances had to be considered. An impedance plot is shown in Fig. 8. The data points fit well to a semicircular least-squares approximation based on an electrical model consisting of a simple resistor–capacitor parallel network in series with an ohmic resistor, a model valid for unilayered epithelia with open lateral spaces [24]. Intersections between the semicircle and the *x*-axis at high and low frequencies signified the series re-

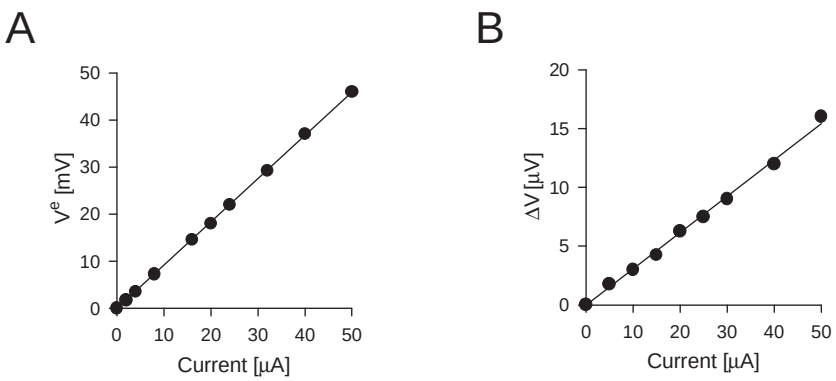

Fig. 7A, B Linearity of response upon variation of amplitude of the current applied in a typical control experiment. **A** Amplitude of transepithelial voltage (V^e) as a function of current amplitude. **B** Scanning signal (Δ*V*), measured 30 μm above the epithelium, as a function of current amplitude

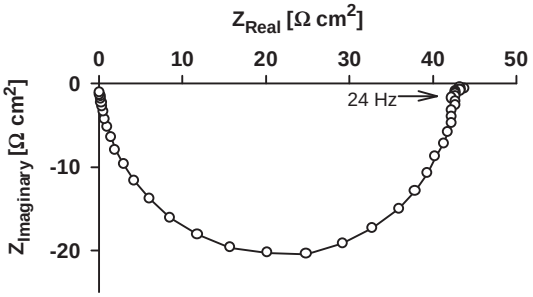

Fig. 8 Characteristic Nyquist plot of the transepithelial impedance of MDCK cell monolayers. The resistance of the filter support had been subtracted. *Abscissa* and *ordinate* give real (ohmic) and imaginary (reactive) components of the complex impedance. *Symbols* are data points measured at given frequencies. The *arrow* denotes impedance at 24 Hz

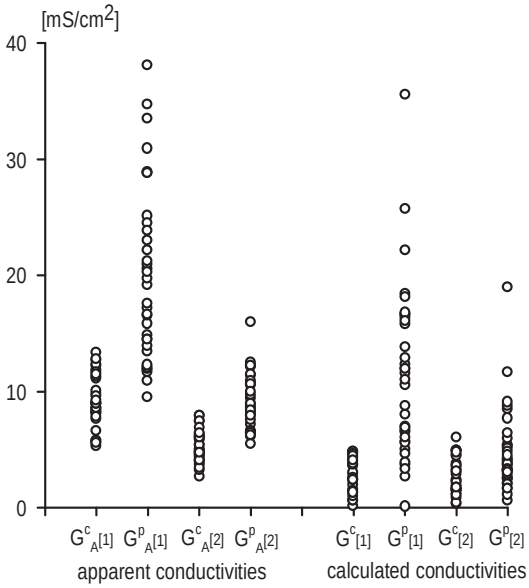

Fig. 9 *Left columns:* apparent conductivities (G_A), referring to gross tissue area, measured above cell centres (*index c*) and above tight junctions (*index p*) without ([1]) or with mucosal-to-serosal sucrose gradient ([2]) of all sites recorded from. Each *point* represents the mean of two to four measurements in the same location. The number of locations (*m*) is given in Table 1. *Right columns:* true trans- and paracellular epithelial conductivities (G^c and G^p) were calculated. The data show a large standard deviation, because measurements of individual points recorded from 10 different tissues are shown together

sistance and the sum of transepithelial and series resistance, respectively. The real component of the impedance at 24 Hz was 45.1 Ω · cm^2 or 99.6% of the (ohmic) epithelial resistance, R_T, of 45.3 Ω · cm^2. The results show that the error caused by using alternating current of 24 Hz was negligible.

Apparent conductivities

Scanning signals recorded above cell centres and above tight junctions were, in the first instance, expressed as apparent conductivities by means of Eq. 1 (Fig. 9 and Table 1). In control Ringer's, as well as with 40 mM sucrose on the mucosal side, there were no non-conductive spots (as described by Cereijido et al. [5]). Above tight junctions the apparent conductivity (G^p_A) was about twice that above the cell centres (G^c_A). With a sucrose gradient, the apparent conductivities decreased at both sites by about half. Since upon addition of sucrose the intercellular spaces shrank, the decreae of the apparent conductivity measured above cell centres indicates that it is strongly affected by the local conductivity of the paracellular pathway. From the plot of G^c_A as a function of G^p_A (Fig. 10) model 3 yielded the true transcellular conductivity, G^c, as 2.6±0.7 mS/cm^2 (20 data points, *n*=10 monolayers).

Table 1 Mean scanning signals above cell centres and tight junctions, presented as apparent trans- and paracellular conductivities, G^c_A and G^p_A, according to Eq. 1. They were measured before (*control*) and after mucosal addition of sucrose (*osmotic gradient*) in 10 experiments. (*m* The number of data points)

Control		Osmotic gradient	
G^c_A (mS/cm^2)	G^p_A (mS/cm^2)	G^c_A (mS/cm^2)	G^p_A (mS/cm^2)
9.2±0.4 *m*=33	20.0±1.3 *m*=35	5.3±0.3 *m*=31	9.1±0.4 m=35

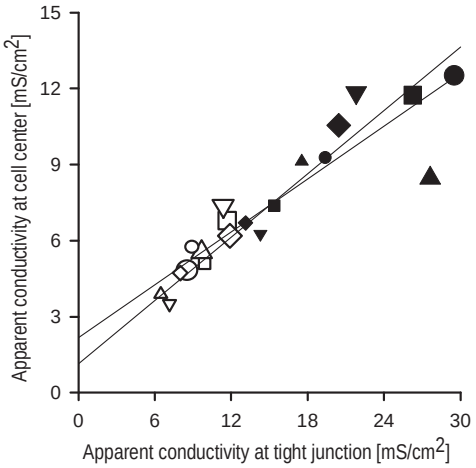

Fig. 10 Mean apparent conductivities at tight junctions (*abscissa*) and cell centres (*ordinate*) measured with (*open symbols*) or without a mucosal-to-serosal sucrose gradient (*filled symbols*) in ten experiments. *Symbols* different in size or form indicate different experiments. In each case was $0<G^c_A<G^p_A$, and both apparent conductivities decreased with the sucrose gradient. Regression lines are shown

Variation of scanning signals

In each experiment, two to four measurements were performed at each spot from which recordings were made; however, after the first measurement, other spots of the epithelial area were investigated before the second and

Table 2 Standard deviation (in %) of individual scanning signals, presented as apparent conductivities, G_A^c and G_A^p, before (*control*) and after mucosal addition of sucrose (*osmotic gradient*). Two cases were considered: (1) repeated measurements from the same cell centre or tight junction, and (2) the first recordings made from different cell centres or different tight junctions in the same epithelial area. (*m* The number of data points, *n* the number of epithelial areas)

	Control		Osmotic gradient	
	%SD (G_A^c)	%SD (G_A^p)	%SD (G_A^c)	%SD (G_A^p)
1. Same location	15.4±2.9	17.7±2.6	15.5±2.3	14.6±1.7
m	33	35	31	35
2. Different locations	12.2±1.8	14.4±1.1	15.1±2.4	11.3±1.4
n	10	10	10	10

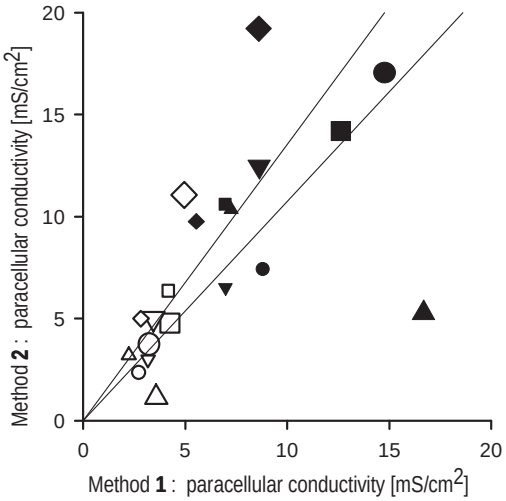

Fig. 11 Paracellular conductivities of ten monolayers (represented by the same symbols as used in Fig. 10) with (*open symbols*) or without a mucosal-to-serosal sucrose gradient (*filled symbols*). The values derived with method 1 and method 2 are indicated on *abscissa* and *ordinate*, respectively. Regression lines are shown

subsequent measurements were made. As a measure of reproducibility of the scanning signals after repositioning the electrode, the standard deviation of repeated measurements on the same spot was determined (Table 2). For measurements made at cell centres or tight junctions and under control conditions or with osmotic gradient, the standard deviation was 13–19% without significant differences between the conditions tested.

In order to assess the heterogeneity of trans- and paracellular conductivities, we evaluated the standard deviation of the first measurements over all cell centres of tight junctions, respectively, in the same epithelial area and under the same condition (Table 2). In each case, the result (10–18%), was not significantly different from the standard deviation of repeated measurements over the same spot. Thus, heterogeneity of trans- or paracellular conductivity was not observed.

Table 3 Trans-(G^c) and paracellular (G^p) conductivities, and their sum, the epithelial conductivity (G^e) under control conditions and under the osmotic gradient, according to the three methods used. Percentages are contributions of paracellular conductivity to total epithelial conductivity. There was no significant difference between respective data of the three models. Differences between controls and osmotic gradient were $P<0.001$

G^c (mS/cm²)	G^p (mS/cm²)		G^e (mS/cm²)	
	Control	Osmotic gradient	Control	Osmotic gradient
Method 1 (*n*=10): 2.5±0.5	9.7±1.2 (81±10%)	3.5±0.3 (56±4%)	12.0±0.9	6.2±0.4
Method 2 (*n*=10): 2.7±0.5	11.3±1.4 (80±10%)	4.6±0.9 (62±12%)	14.0±1.3	7.3±0.7
Method 3 (*n*=10): 2.6±0.7				

True conductivities

G^c and G^p were calculated using the models described above. The application of averaged model parameters to single scanning signals (Fig. 9, right) provides the only assessment of individual trans- and paracellular conductivities so far available. Transcellular conductivities were significantly lower than paracellular ones. The G^p values derived from methods 1 and 2 correlated well in eight of ten experiments (Fig. 11).

According to models 1 and 2, mean G^c was 2.5±0.5 (n=10) or 2.7±0.5 mS/cm² (n=10; n.s.), respectively (Table 3). The mean G^p was 9.7±1.2 (n =10) or 11.3±1.4 mS/cm² (n=10; n.s.) without an osmotic gradient, and 3.5±0.3 (n=10) or 4.6±0.9 mS/cm² (n=10; n.s.) with an osmotic gradient. The excellent agreement of the values achieved using the different models corroborated the validity of the assumptions made. Under control conditions G^p was predominantly determined by the barrier of the tight junctions, while under the osmotic gradient the resistance of intercellular spaces contributed, so that G^p was reduced to 40% of the control value. Control epithelial conductivity was reduced under the sucrose gradient by almost half. As G^p was four times higher than G^c, confluent MDCK monolayers of clone C11 can be classified as leaky epithelia.

Superposition of trans- and paracellular currents

The superposition of local trans- and paracellular currents can be expressed by Eqs.2 and 3 (see Materials and methods). The mean relative contributions of the paracellular pathway to the scanning signals measured above cells and junctions were k_1=0.75 and 0.61 in models 1 and 2, respectively, and k_2=1.8 in both models. These parameters do not depend on the magnitude of the conductivities but only on the geometrical distribution of the conductivities, i.e.size and shape of the cells in the area

explored. Clearly, k_1 could not be neglected. Because G^p was four times G^c, it contributed more to the scanning signal measured above the cells compared with G^c.

Discussion

As early as 1972, Frömter introduced, in his pioneering study [10], the voltage-scanning technique using microelectrodes to measure, with fine discrimination, potential gradients induced above cell surfaces and tight junctions while current is passed through the epithelium. The apparent conductivity G_A^p, calculated using Eq. 1 from the scanning signal measured above tight junctions, cannot (as in [5]) be interpreted as the conductance per unit surface of junction, because: (1) the diameter of the microelectrode is not small enough compared to the diameter of the tight junction; and (2) the scanning signal is not equal to the electric field at the tight junction, because the distance, Δx, traversed by the vertical steps of the scanning microelectrode is not small enough compared to the field distortion near the tight junction (Fig. 4). The present study showed that, because of the superposition of trans- and paracellular currents, apparent conductivities are not suitable estimates of the true conductivities. This problem was solved by establishment of mathematical models and by improvements of resolution and sensitivity of the experimental technique. Insignificant differences of the results produced with different models indicate the validity of the assumptions made.

Resolution and sensitivity

The competing vibrating probe technique achieves high sensitivity and a temporal resolution of <1 s. But according to our theoretical analysis, the spatial resolution is not sufficient for differentiation between trans- and paracellular pathways, because the large probe (diameter about 6 μm) must be kept at least 7 μm distant from the epithelial surface, and the position of the probe is precise by only ±3μm [8, 28]. Because of the sub-micrometre resolution, microelectrode scanning techniques are superior in the present application. Nevertheless the precision of single measurements was limited by the spatial resolution achieved, rather than the sensitivity of the recording system.

Using a microelectrode voltage-scanning technique and studying low-resistance non-differentiated MDCK monolayers, Cereijido et al. [5] considered apparent conductivities above cell membranes and junctions. The authors found that cell bodies are never conductive, and also in half of the paracellular sites conductivity was not detected. The authors conclude that the terminal bars are functionally tight along 50% of their lengt. In contrast, the present study found a significant apparent conductivity in all spots recorded from, albeit G_A^p was higher than G_A^c. This discrepancy can be understood when the improved sensitivity (about 1 mS/cm^2) is considered. The findings of Cereijido et al. are conceivable, if the sensitivity of their method is about 15 mS/cm^2 (about 10 mS/cm^2 is estimated by the authors), because then the apparent transcellular conductivities and half of the paracellular ones are below the experimental resolution.

Conductivities of MDCK-C11 monolayers

The conductivity of confluent MDCK-C11 monolayers (13 mS/cm^2), measured in buffered electrolyte solution, was higher than that (3 mS/cm^2) measured by Gekle et al. [11] in C11 monolayers (62–72 passages, similar to the present study) grown on permeable membrane filters, which were bathed in MEM culture medium. In the latter study the standard deviation (70%) was higher than that in the present experiments (27%). Variation of epithelial conductivities is, however, often observed in studies of cultured monolayers. Barker and Simmons [3] and Hein et al. [13] measured 10–20 mS/cm^2 in strain II MDCK cells, cultured on membrane filters that were bathed in phosphate–buffered saline or modified Krebs' solution. High conductivities were also measured in the wild-type MDCK monolayers studied in culture medium without serum or in Hanks' balanced salt solution (4–21 days after plating on membrane filters) by Misfeldt et al. [20], who measured 12 mS/cm^2. In monolayers of wild-type cells (plated on nylon cloth coated with collagen and bathed in culture medium), Cereijido et al. [5] and Stefani and Cereijido [30] found conductivities of 3–14.3 mS/cm^2, which decreased with the number of passages.

As a result of our study, confluent MDCK-C11 monolayers can be classified as leaky epithelia, because the paracellular pathway was about four times more permeable than the transcellular pathway. The transcellular conductivity (2.6 mS/cm^2) must be higher than that of high-resistance MDCK monolayers, where the resistance sets an upper limit of 0.2–0.5 mS/cm^2 to the transcellular conductivity [3, 4, 11], similar to results of Kottra [14] in a study of *Necturus* gallbladder. The relatively high transcellular conductivity of MDCK-C11 cells may possibly be explained by a large Cl^- conductance in the apical membrane [11]. Since the transference numbers of the tissue for Na^+ is only twice as high as that for Cl^- [21, 22], cation selectivity of the tight junctions implies transcellular Cl^- flux. In rabbit salivary duct epithelia, the high conductivity (about 100 mS/cm^2 in symmetrical 150 mM Cl^-) resides in the cell membrane and is not due to a paracellular pathway [1]. Furthermore, at least in mucosal-to-serosal Na^+ fluxes, the transcellular pathway can contribute significantly in low-resistance MDCK cells [17].

In MDCK cells, a Cl^- conductance is activated during volume regulation [23]. Unless exposed to adrenaline, however, hyperosmotic exposure of the apical surface of Cl^--secreting MDCK epithelia does not result in pronounced effects upon short-circuit currents [26], suggesting that the apical Cl^- conductance, and hence also the transcellular pathway, is not changed by mucosal addi-

tion of sucrose. Moreover, the good agreement of calculations based on model 1 (where the osmotic perturbation is not required) and models 2 and 3 supports the assumption of sucrose affecting predominantly the paracellular pathway. Using alternating current spectroscopy, Kottra [14] has shown that in *Necturus* gallbladder exposed to hyperosmotic mucosal Ringer's solution the paracellular resistances of both tight junctions and lateral intercellular spaces increase and that the resistance of the apical membrane remains unchanged.

Repeated measurements over the same tight junction had the same standard deviation as measurements over different tight junctions. Thus, in contrast to previous findings [5] there was no evidence of a heterogeneously distributed conductivity in the tight junctions.

Resistance of lateral intercellular spaces

Mucosal addition of sucrose can decrease paracellular and transepithelial conductivities, because intercellular spaces shrink [14, 18, 33]. In the present study, the osmotically induced increase of the transepithelial resistance was larger than the 45% increase observed by Misfeldt et al. [20]. Under control conditions, i.e. with dilated intercellular spaces, the paracellular resistance was dominated by the resistance of the tight junctions. With collapsing intercellular spaces, however, the paracellular resistance increased. The present findings support the idea that the width of the lateral intercellular spaces can, under special conditions, mediate the permeability through the paracellular route, and are thus in accordance with results of Smulders et al. [27] which indicate that the contribution of the lateral spaces to the resistance of rabbit gallbladder may be signicant only during osmotically induced serosal-to-mucosal water flux. The impedance measurements of Kottra and Frömter [15] show that in *Necturus* gallbladder epithelium under control conditions the resistance of tight junctions is 3.5 times larger than that of the lateral intercellular spaces, but after collapse of the spaces their resistance exceeds that of the junctions.

Acknowledgements This work was supported by the Deutsche Forschungsgemeinschaft (DFG Fr-652/3-3). MDCK cells were a kind gift of Professor H. Oberleithner. Electronic circuitry was composed by Dipl.-Ing. D. Sorgenfrei. The authors thank Professor C.J. Bentzel for valuable suggestions. Last, but not least, the expert technical assistance of S. Lüderitz is gratefully acknowledged.

Appendix

Method 1 required calculation of the supraepithelial electric field that fitted the potential differences recorded. Theoretical approaches to this type of electrodynamical problem are based on Poisson's equation and the Nernst-Planck electroneutrality condition [16, 31]. Closed form solutions are not available in cases of practical importance, because the boundary conditions are inhomogeneous. In order to accelerate the numerical analysis, we sought a simple mathematical formulation.

In the geometrical representation described above, the surface cell has two orthogonal symmetry axes of rotation (Fig. 2). This reduced the number of computations. The dimensions of bulk elements were chosen such that the conductance between a bulk element and its neighbour, g, was the same for all bulk elements and all faces of each bulk element:

$$g = \sin(60°) \cdot L_a/(\rho \cdot n_a^2) \quad (14)$$

where ρ is the specific resistivity of the electrolytic bath solution, and L_a and n_a are the length of a side of the surface cell and the number of surface elements in each side of the surface cell, respectively, as defined in the text. (Lower-case letters are used for symbols referring to surface or bulk elements).

According to the principle of charge conservation in a stationary or quasi-stationary state, the sum of the electric current flowing into a rhombohedral bulk element must equate to zero. For all bulk elements, except for those next to the epithelium, we therefore have:

$$\sum \Delta v_f = 0 \quad (f = 1 \ldots 6) \quad (15)$$

where Δv_f is the potential difference between the bulk element and its neighbour at face f. For bulk elements next to the epithelium, the current i_s flowing through the face (f=6) looking to the adjacent epithelial surface element (s) must be considered. The paracellular contribution to i_s was assumed to be proportional to the length of tight junction in the surface element s, so that:

$$i_s = \sin(60°) \cdot L_a^2 \cdot V^e \cdot (r_s \cdot G^p) + (G^c/n_a^2), \quad (16)$$

where $\sin(60°) \cdot L_a^2$ is the area of the surface cell, and r_s is the ratio of the length of tight junction in the surface element s over the total length of tight junction in the surface cell. For the bulk elements next the epithelium, we obtain:

$$\sum \Delta v_f + i_s/g = 0 \quad (f = 1 \ldots 5) \quad (17)$$

In the top layer of bulk cells (at distance L_b from the epithelium), where potential differences in the horizontal plane (i.e. the plane parallel to the epithelial surface) vanish, the electric potential was set at zero. The translational symmetry of the surface cell (Fig. 2) implicates that two bulk cells in the same horizontal plane are interchangeable if the values of a horizontal coordinate are congruent, modulo n_a. This allowed computation of Δv_f if the two adjoining bulk cells were in different surface cells. The boundary condition Δv_f=0 applied if the bulk element's neighbour at face f was occupied by the glass electrode.

After an educated guess of G^c and G^p, Eqs. 15 and 17 were solved numerically by systematic variation of the potential in each bulk element. By comparison of the resulting supraepithelial potential distribution with the potential differences measured, G^c and G^p were determined in a conventional fit routine (Fig. 3)

References

1. Augustus J, Bijman J, van Os CH (1978) Electrical resistance of rabbit submaxillary main duct: a tight epithelium with leaky cell membranes. J Membr Biol 43:203–226
2. Bakker R, Dekker K, DeJonge HR, Groot JA (1993) VIP, serotonin, and epinephrine modulate the ion selectivity of tight junctions of goldfish intestine. Am J Physiol 264:R362–R368
3. Barker G, Simmons NL (1981) Identification of two strains of cultured MDCK renal epithelial cells which display entirely different physiological properties. Q J Exp Physiol 66:61–72
4. Brown CDA, Simmons NL (1981) Catecholamine stimulation of Cl^- secretion in MDCK epithelium. Biochim Biophys Acta 649:427–435
5. Cereijido M, Stefani E, Martinez-Palomo A (1980) Occluding junctions in a cultured transporting epithelium: structural and functional heterogeneity. J Membr Biol 53:19–32
6. Fallon ME, Brecher MA, Balda MS, Matter K, Anderson JM (1995) Altered hepatic localization and expression of occludin after common bile duct ligation. Am J Physiol 269:C1057–C1062
7. Fasano A, Baudry B, Pumplin DW, Wasserman SS, Tall BD, Ketley JM, Kaper JB (1991) Vibrio cholerae produces a second enterotoxin, which affects intestinal tight junctions. Proc Natl Acad Sci USA 88:5242–5246
8. Foskett JK, Scheffey C (1989) Scanning electrode localization of transport pathways in epithelial tissues. Methods Enzymol 171:792–813
9. Fromm M, Palant CE, Bentzel CJ, Hegel U (1985) Protamine reversibly decreases paracellular cation permeability in *Necturus* gallbladder. J Membr Biol 87:141–150
10. Frömter E (1972) The route of passive ion movement through the epithelium of *Necturus* gallbladder. J Membr Biol 8:259–301
11. Gekle M, Wünsch S, Oberleithner H, Silbernagl S (1994) Characterization of two MDCK-cell subtypes as a model system to study principal cell and intercalated cell properties. Pflügers Arch 428:157–162
12. Hecht G, Koutsouris A, Pothoulakis C, LaMont JT, Madara JL (1992) Clostridium difficile toxin B disrupts the barrier function of T84 monolayers. Gastroenterology 102:416–423
13. Hein M, Madefessel C, Haag B, Teichmann K, Post A, Galla HJ (1992) Implications of a non-lamellar lipid phase for the tight junction stability. Part II: reversible modulation for transepithelial resistance in high and low resistance MDCK-cells by basic amino acids, Ca^{2+}, protamine and protons. Chem Phys Lipids 63:223–233
14. Kottra G (1991) Elektrophysiologische Untersuchungen der Zellmembranen und der parazellulären Shunts am Gallenblasenepithel von *Necturus maculosus* (Gefleckter Furchenmolch) mit einem neuartigen Verfahren der Impedanzanalyse. Habil Thesis, University of Frankfurt/Main Medical School
15. Kottra G, Frömter E (1984) Rapid determination of intraepithelial resistance barriers by alternating current spectroscopy. II. Test of model circuits and quantification and results. Pflügers Arch 402:421–432
16. Kottra G, Weber G, Frömter E (1989) A method to quantify and correct for edge leaks in Ussing chambers. Pflügers Arch 415:235–240
17. Kovbasnjuk O, Chatton JY, Friauf WS, Spring KR (1995) Determination of the Na permeability of the tight junctions of MDCK cells by fluorescence microscopy. J Membr Biol 148: 223–232
18. Loeschke K, Bentzel CJ (1994) Osmotic water flow pathways across *Necturus gallbladder*: role of the tight junction. Am J Physiol 266:G722–G730
19. Madin SH, Darby NB (1958) As catalogued in: American Type Culture Collection catalogue of strains, vol 2. ATCC Books, Waldorf, MD, USA, pp 574–576
20. Misfield DS, Hamamoto ST, Pitelka DR (1976) Transepithelial transport in cell culture. Proc Natl Acad Sci USA 73:1212–1216
21. Oberleithner H, Vogel U, Kersting U (1990) Madin-Darby canine kidney cells. I. Aldosterone-induced domes and their evaluation as a model system. Pflügers Arch 416:526–532
22. Oberleithner H, Vogel U, Kersting U, Steigner W (1990) Madin-Darby canine kidney cells.II. Aldosterone stimulates Na^+/H^+ and Cl^-/HCO_3^- exchange. Pflügers Arch 416:533–539
23. Paulmichl M, Friedrich F, Maly K, Lang F (1989) The effect of hypoosmolarity on the electrical properties of Madin Darby canine kidney cells. Pflügers Arch 413:456–462
24. Schifferdecker E, Frömter E (1978) The AC impedance of *Necturus* gallbladder epithelium. Pflügers Arch 377:125–133
25. Schulzke JD, Schulzke I, Fromm M, Riecken EO (1995) Epithelial barrier and ion transport in coeliac sprue: electrical measurements on intestinal aspiration biopsies. Gut 37:777–782
26. Simmons NL, Tivey DR (1992) The effect of hyperosmotic challenge upon ion transport in cultured renal epithelial layers (MCK). Pflügers Arch 421:503–509
27. Smulders A, Tomey JM, Wright EM (1972) The effect of osmotically induced water flows on the permeability and ultrastructure of the rabbit gallbladder. J Membr Biol 7:164–197
28. Somieski P, Shipley A, Nagel W (1996) Vibrating probe analysis of voltage-activated chloride current across amphibian skin. Pflügers Arch 431:R96
29. Spitz J, Yuhan R, Koutsouris A, Blatt C, Alverdy J, Hecht G (1995) Enteropathogenic *Escherichia coli* adherence to intestinal epithelial monolayers diminishes barrier function. Am J Physiol 268:G374–G379
30. Stefani E, Cereijido M (1983) Electrical properties of cultured epithelioid cells (MDCK). J Membr Biol 73:177–184
31. Sten-Knudsen (1978) Passive transport processes. In: Giebisch G, Tosteson DC, Ussing HH (eds) Membrane transport in biology,vol 1. Springer, Berlin Heidelberg New York, pp 5–140
32. Valentich JD (1981) Morphological similarities between the dog kidney cell line and the mammalian cortical collecting tubule. Ann NY Acad Sci 372:384–405
33. Wiedner G, Wright EM (1975) The role of the lateral intercellular spaces in the control of ion permeation across the rabbit gall bladder. Pflügers Arch 358:27–40
34. Wünsch S, Gekle M, Kersting U, Schuricht B, Oberleithner H (1995) Phenotypically and karyotypically distinct Madin-Darby Canine Kidney cell clones respond differently to alkaline stress. J Cell Physiol 164:164–171